Supporting Information: Nonequilibrium H/D Isotope Effects from Trajectory-based Nonadiabatic Dynamics

Lasse Spörkel, Ganglong Cui*, Axel Koslowski, and Walter Thiel*

October 1, 2013

Email: ganglong@kofo.mpg.de and thiel@kofo.mpg.de

Max-Planck-Institut für Kohlenforschung, Kaiser-Wilhelm-Platz 1, 45470 Mülheim an der Ruhr, Germany

Table of Contents

1 Electronic Structure Calculations

All semiempirical calculations were performed using the OM2/MRCI method, [1–3] as implemented in the MNDO99 code. [4] During optimizations, all required energies and gradients were computed analytically. Minimum-energy conical intersections were located using the Lagrange-Newton approach. [5]

The half-electron restricted open-shell Hartree-Fock (HF) formalism [6] was applied in the self-consistent field (SCF) treatment (i.e., the orbitals were optimized for the leading configuration of the S_1 state with two singly occupied orbitals). The active space in the multi-reference configuration interaction (MRCI) calculations included 12 electrons in 12 orbitals. In terms of the SCF configuration, it comprised the five highest doubly occupied orbitals, the two singly occupied orbitals, and the five lowest unoccupied orbitals. For the MRCI treatment, three configuration state functions were chosen as references, namely the SCF configuration and the two closed-shell configurations derived therefrom (i.e., all singlet configurations that can be generated from the HOMO and LUMO of the closed-shell ground state). The MRCI wavefunction was built by allowing all single and double excitations from these three references. This semiempirical OM2/MRCI approach has been recently shown to perform well in a comprehensive general evaluation of excited-state properties [7] and in a number of recent excited-state studies. [8–20]

Ground-state geometries were also optimized using density functional theory (DFT) calculations with the hybrid B3LYP exchange-correlation functional [21–23] and the 6-31G* basis set. [24] Vertical excitation energies were calculated at these structures using the linear-response TD-DFT (time-dependent DFT) approach, the B3LYP [21–23] and CAM-B3LYP [25] functionals, and the 6-31++G** basis set. [26]

The parameterized, DFT-based multi-reference configuration interaction (DFT/MRCI) method [27] was also used to calculate the vertical excitation energies. To be consistent with the original parameterization, the hybrid BHLYP functional [23] and the TZVP basis set [28, 29] were employed in the DFT/MRCI calculations.

In addition, the complete-active-space self-consistent field (CASSCF) method was applied to optimize the ground- and excited-state structures and to scan the relevant potential energy profiles. In the CASSCF calculations, an active space of ten electrons in eight orbitals was adopted. The multi-state CASSCF second-order perturbation method (CASPT2) [30] was employed to determine improved single-point energies at all CASSCF structures. The MS-CASPT2 calculations were done using two roots with equal weights and the imaginary shift technique (0.3 a.u.). [31]

The following codes were used for the electronic structure calculations in this work: ChemShell 3.4 [32] and MNDO99 [4] for OM2/MRCI; GAUSSIAN09 [33] for DFT, TD-DFT, and minimum-energy conical intersection optimizations (CASSCF); MOLCAS 7.6 [34, 35] for CASSCF and MS-CASPT2; and TURBOMOLE 5.7.1 [36] for DFT/MRCI. [27]

Table 1: The Number of Trajectories that (a) Undergo ESIPT, (b) Decay to the S_0 State, and (c) Remain in the S_1 State until the End of the Simulation.

Temperature (T)	Total	ESIPT	S_0	S_1	Total	ESIPT	S_0	S_1
	7PyIn-H				7PyIn-D			
All	632	626	569	63	735	714	631	104
T < 275 K	219	216	202	17	344	335	300	44
275 K < T < 325 K	251	249	218	33	253	245	217	36
T > 325 K	162	161	149	13	138	134	114	24

2 Dynamics Simulations

In trajectory surface hopping dynamics, there are two main initial-condition sampling schemes. The first one is Wigner sampling, [37, 38] which generates initial coordinates and velocities based on classical or quantum harmonic vibrational modes. The second one is based on canonical classical molecular dynamics (MD). The canonical distribution is satisfied with the use of thermostat algorithms, such as velocity rescaling [39], the Berendsen thermostat, [40] the Andersen thermostat, [41] the Nose-Hoover thermostat, [42, 43] Nose-Hoover chains, [44] or Langevin dynamics [45]. Here, we adopted the Nose-Hoover chains algorithm (with a chain length of 10) for this purpose. We used the default characteristic time of 0.5 ps for the thermostat and a timestep of 1 fs for nuclear motion.

For both target molecules (7PyIn and the deuterated isotopomer 7PyIn-D), ground-state MD runs were performed at the SCC-DFTB level: [46–48] 7 ps of equilibration dynamics were followed by a 10 ps production run, from which 1000 initial atomic coordinates and velocities were randomly selected. The starting points for the subsequent OM2/MRCI nonadiabatic dynamics runs were chosen from this set on the basis of the computed $S_0 \rightarrow S_1$ transition probabilities. A total of 834 [820] surface-hopping trajectories were run up to 2 ps for 7PyIn [7PyIn-D], with all relevant energies, gradients, and nonadiabatic coupling vectors being computed on-the-fly as needed. For points with an S_1 – S_0 energy gap of less than 10 kcal/mol, the fewest-switches criterion was applied to decide whether to hop. [49, 50] The time step was chosen to be 0.1 fs for nuclear motion and 0.0005 fs for electronic propagation. The unitary propagator evaluated at the middle point was used to propagate electronic motion. [51, 52] Translational and rotational motions were removed in each step. The empirical decoherence correction (0.1 au) proposed by Granucci et al. was employed. [53] The final evaluations were done for the 632 [735] trajectories (see Table 1) that finished successfully and satisfied our energy continuity criterion (no changes greater than 30 kcal/mol between any two consecutive MD steps). To analyze the effect of thermal fluctuations on the photodynamics of 7PyIn and 7PyIn-D, the trajectories were apportioned into three temperature windows according to the initial conditions. Further technical details are given in our previous publications. [8–20, 51, 52] The SCC-DFTB sampling with the Nose-Hoover chains technique was done with ChemShell 3.4 [32] and the nonadiabatic OM2/MRCI dynamics simulations were conducted with MNDO99. [4]

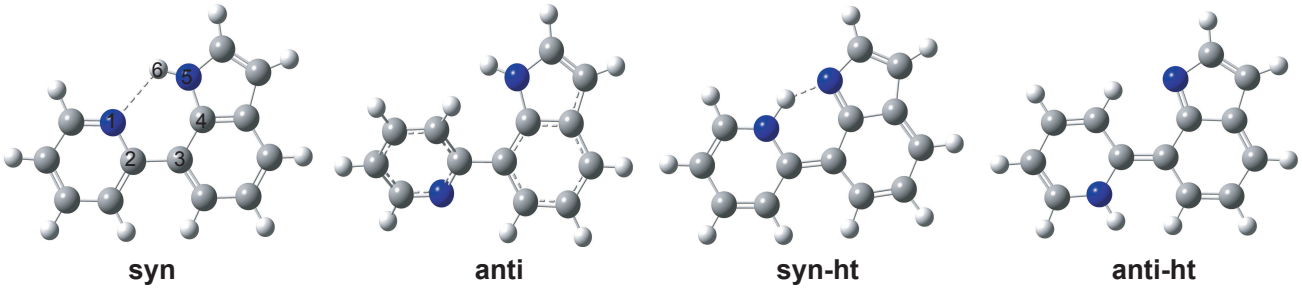

Figure 1: Schematic ground-state geometries optimized in this work. In the S_0 state, the syn conformer is most stable. Also shown for syn is the chosen numbering scheme.

Table 2: Selected Geometric Parameters and Relative Energies of the Optimized Structures Obtained from OM2/MRCI, B3LYP and CASSCF

	N1-H6 (Å)	N5-H6 (Å)	C2-C3 (Å)	N1-C2-C3-C4 (°)	Energies (kcal/mol)
OM2/MRCI					
S0-syn	2.14	1.01	1.48	0.0	0.0
S0-anti	4.10	1.01	1.49	140.3	3.0
S0-anti-ht	1.02	4.93	1.43	179.9	49.4
S1-syn	1.90	1.04	1.44	0.0	96.3
B3LYP/6-31G*					
S0-syn	2.09	1.01	1.48	0.0	0.0
S0-syn-ht	1.11	1.53	1.44	0.0	17.8
S0-anti	4.18	1.01	1.48	148.3	5.9
S0-anti-ht	1.01	4.92	1.43	179.8	34.4
MS-CASPT2/6-31G*//CASSCF(10,8)/6-31G*					
S0-syn	2.18	0.99	1.49	0.0	0.0
S1-syn	1.91	1.01	1.43	0.0	99.9

The results from the static electronic structure calculations are of course identical for 7PyIn and 7PyIn-D since the nuclear masses do not enter the electronic Hamiltonian. In the dynamics simulations, the atomic mass of the H6 (D6) atom in 7PyIn (7PyIn-D) was assigned to be 1.008 (2.014) amu. This small mass difference has a remarkable influence on the photodynamics.

3 S_0 Minima and Potential Energy Profiles

In the ground state there are four possible conformers (see Fig. 1), which are referred to as syn, anti, syn-ht, and anti-ht, respectively. The lowest among them is the syn conformer that is more stable than the anti conformer by 5.9 kcal/mol at the B3LYP/6-31G* level and 3.0 kcal/mol at the OM2/MRCI level (see Table 2 and the right panel of Fig. 2). Hydrogen transfer of H6 in the syn arrangement yields the syn-ht tautomer. At the B3LYP/6-31G* level, it lies 17.8 kcal/mol above the syn conformer; a scan of the S_0 potential energy profile along the hydrogen transfer shows that syn-ht is metastable and occupies a very shallow potential well (with a lowest harmonic frequency of only 78 cm^{-1}). At the OM2/MRCI level, there is no syn-ht minimum: all geometry optimization

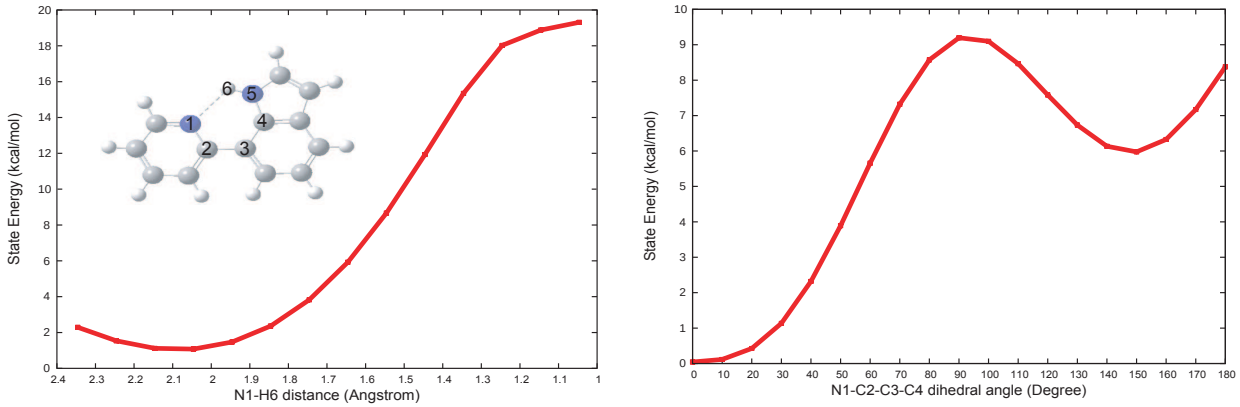

Figure 2: B3LYP/6-31G* energy profiles for one-dimensional relaxed minimum-energy paths along the N1-H6 bond length (left) and the N1-C2-C3-C4 dihedral angle (right).

attempts starting from a syn-ht-type structure ended up back at the syn conformer. Finally, the anti-ht conformer is dynamically unimportant because of its very high potential energy, 34.4 kcal/mol at the B3LYP/6-31G* level and 49.4 kcal/mol at the OM2/MRCI level.

4 Absorption Spectrum

To investigate the excited states in the Franck-Condon region, the vertical absorption spectrum of the S0-syn conformer was computed at the TD-DFT/6-31++G**//B3LYP/6-31G* level using the B3LYP, CAM-B3LYP, and M06-2X exchange-correlation functionals. The spin-allowed $S_0 \rightarrow S_1$ electronic transition is found to give rise to the strongest absorption band (see Fig. 3). This excited singlet state is of partial charge-transfer character so that the conventional global hybrid functional B3LYP underestimates the excitation energy by ca. 0.5 eV, compared with range-separated (CAM-B3LYP) and modern (M06-2X) functionals. The latter give vertical excitation energies (4.06–4.08 eV) that are close to the values from DFT/MRCI (3.95 eV), and CC2 (4.0 eV), but lower than those from OM2/MRCI (4.37 eV) and MS-CASPT2//CASSCF (4.34 eV).

5 Conical Intersections

Conical intersections play a central role in nonadiabatic dynamics simulations. The chosen electronic structure method must therefore be able to describe conical intersections reasonably well.

Table 3 lists selected geometric parameters for conical intersection structures obtained from OM2/MRCI and CASSCF. The SA2-CASSCF/6-31G* optimization yields a twisted structure with an N1-C2-C3-C4 dihedral angle of 68° and an N5-H6 distance of 2.55 Å that indicates a weak hydrogen bonding interaction. The energy of this structure relative to the ground-state minimum is 84.3 kcal/mol at the CASSCF level. Single-point MS-

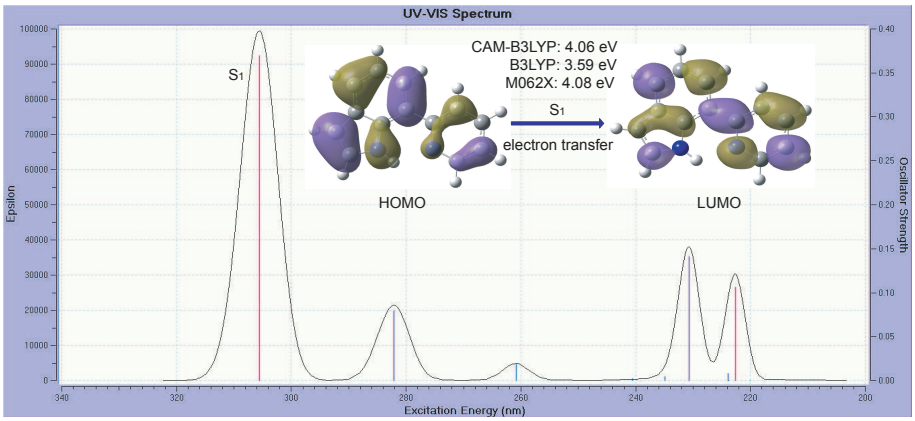

Figure 3: Absorption spectrum (half-width at half height: 0.05 eV) from CAM-B3LYP/6-31++G**//B3LYP/6-31G* calculations.

Table 3: Selected Geometric Parameters and Relative Energies of the Optimized Conical Intersections Obtained from OM2/MRCI and CASSCF (see text)

	N1-H6 (Å)	N5-H6 (Å)	C2-C3 (Å)	N1-C2-C3-C4 (°)	Energies (kcal/mol)
OM2/MRCI					
S1S0-MECI-1	1.06	2.03	1.50	50.4	78.8
S1S0-MECI-2	1.05	2.15	1.49	56.6	78.8
S1S0-MECI-3	1.02	2.92	1.48	67.7	82.6
S1S0-MECI-4	1.02	3.50	1.48	90.4	77.3
CASSCF(10,8)/6-31G*					
S1S0-MECI	1.00	2.55	1.49	63.2	84.3

CASPT2/6-31G* calculations lead to a splitting of the two degenerate CASSCF states, with energies of 67.0 and 77.6 kcal/mol.

At the OM2/MRCI level, we find that the optimizations converge to conical intersection structures with different N1-C2-C3-C4 dihedral angles and N5-H6 distances depending on the N1-C2-C3-C4 value in the starting geometry and on the chosen convergence criteria. Table 3 lists four such structures with varying degrees of hydrogen bonding (see N5-H6 distance). Their energies are rather similar (77.3–82.6 kcal/mol) and lie in the range of the MS-CASPT2/6-31G* and CASSCF/6-31G* values (see above). The lowest-energy species S1S0-MECI-4 has a perpendicular conformation without N5-H6 hydrogen bonding (at 77.3 kcal/mol). In the main paper, we refer to this species as the S1S0-MECI from OM2/MRCI.

To summarize, the OM2/MRCI approach yields a rather extended conical intersection region, with similar energies for N1-C2-C3-C4 dihedral angles between 50° and 90°. The S1S0-MECI obtained from CASSCF is embedded into this region in terms of its structure, and the corresponding CASSCF and MS-CASPT2 single-point energies are of similar magnitude as the OM2/MRCI values.

6 S_1 Minimum-Energy Profiles

Figs. 4–6 show the minimum-energy profiles along the relevant reaction paths at the MS-CASPT2//CASSCF, CASSCF, and OM2/MRCI levels, respectively, obtained at the optimized S_1 geometries (full relaxation of all degrees of freedom except for the reaction coordinate). The left panels depict the potential energy profiles for ESIPT using the distance N1-H6 of the forming covalent bond as the reaction coordinate. The shape of these curves is similar at all three levels: the optimized S_1 energies stay roughly at a plateau down to an N1-H6 distance of 1.6 Å and then drop as the covalent N1-H6 bond is formed, while the single-point S_0 energies go through a maximum at ca. 1.2 Å but always remain below their S_1 counterparts. In absolute terms, the S_1 energies are highest for CASSCF, the inclusion of dynamic correlation in CASPT2 causes a downward shift of ca. 10 kcal/mol, and the OM2/MRCI results are still somewhat lower (by ca. 5-10 kcal/mol). The right panels of Figs. 4–6 display the S_1 and S_0 potential energy profiles along the N1-C2-C3-C4 dihedral angle, which provide the link to the S_1/S_0 conical intersection. On these pathways, the conical intersection is encountered at a N1-C2-C3-C4 dihedral angle of ca. 70° for CASSCF and ca. 80° for OM2/MRCI; it becomes an avoided crossing at the MS-CASPT2 level. During the approach to the conical intersection region, the S_1 profiles remain rather flat in all cases (with barriers not exceeding 2 kcal/mol), while the S_0 profiles show a monotonous increase of ca. 15–25 kcal/mol. Overall, the OM2/MRCI curves are similar enough to their CASSCF and MS-CASPT2 counterparts to support the use of the OM2/MRCI method in the nonadiabatic simulations (see Figs. 4–6).

Finally, we note that analogous energy profiles have been published previously at the CC2/cc-pVDZ level for geometries optimized at MP2/SV(P) (S_0) and CC2/SV(P) (S_1), see Figure 12 of Ref. [54]. The shapes of these profiles are qualitatively similar to those shown here. It should be noted in this context that the S_1 energy profile for ESIPT in Ref. [54] seems to drop off significantly faster than those presented here. This is due to the fact that the S_1 curve in Ref. [54] refers to a different reaction coordinate, i.e. the distance N5-H6 of the covalent bond being broken (rather than the distance N1-H6 chosen here); we have confirmed that the OM2/MRCI curve for the S_1 ESIPT process also drops off fast when using N5-H6 as reaction coordinate (like in the CC2 case, data not shown).

7 Nonequilibrium H/D Isotope Effects

Nonequlibrium H/D isotope effects may occur in chemical reactions when thermodynamic equilibrium is not achieved before the reaction is complete, for example in the case of ultrafast excited-state proton transfer.

From the present dynamics simulations, we can determine the time required for the ESIPT process in each trajectory. We have adopted the geometric criterion to measure the ESIPT time at the point when the distance in the breaking N5-H6 bond exceeds 1.5 Å. The corresponding ESIPT time distributions for 7PyIn and 7PyIn-D

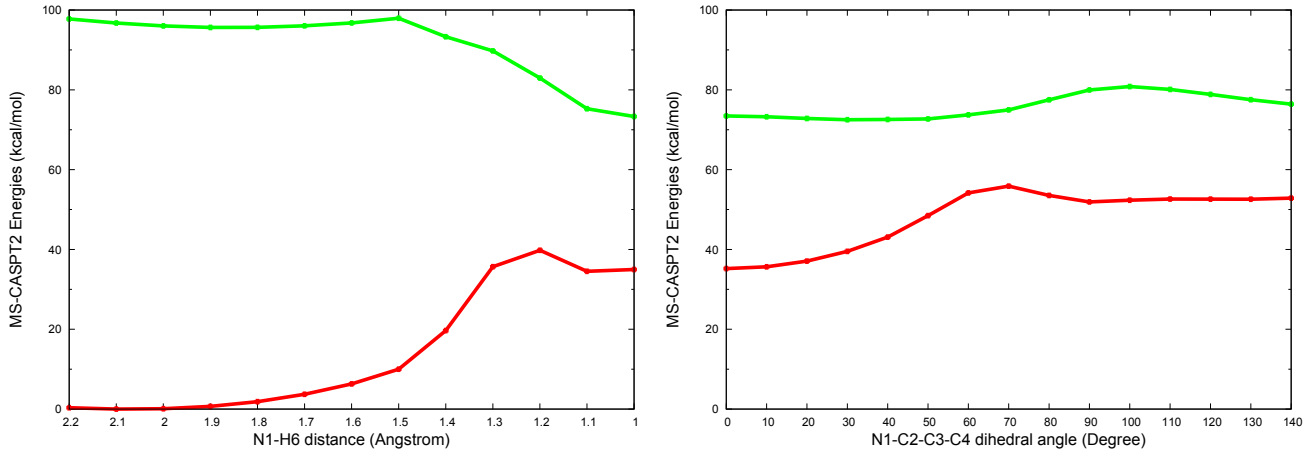

(a) (b)

Figure 4: MS-CASPT2/6-31G*//SA3-CASSCF(10,8)/6-31G* energy profiles for relaxed one-dimensional minimum-energy paths (MEPs) along the N1-H6 bond length (left) and the N1-C2-C3-C4 dihedral angle (right). The S_1 MEP is fully optimized with respect to the other coordinates at the CASSF level, while the S_0 curve is obtained from single-point calculations.

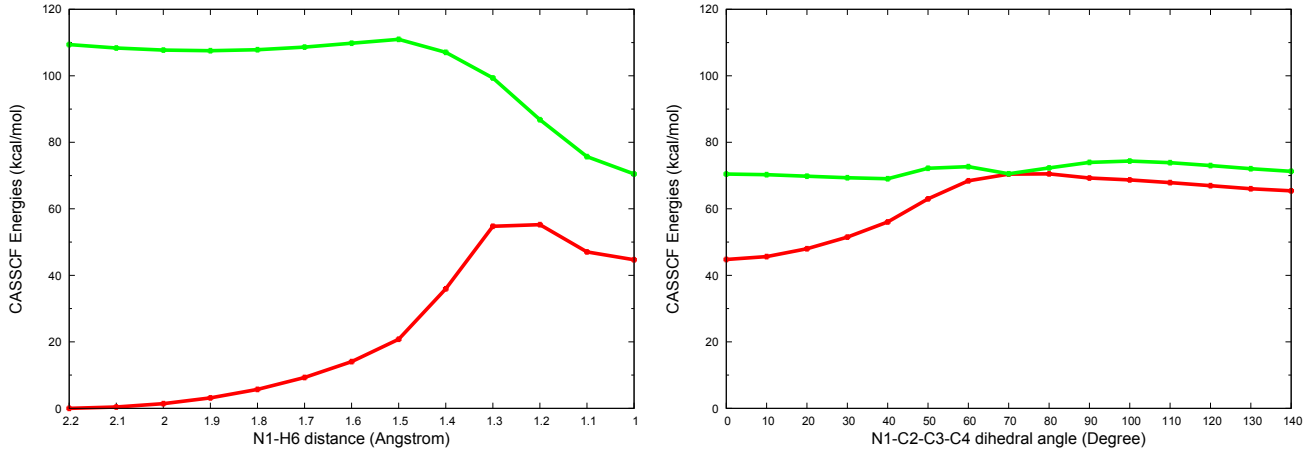

(a) (b)

Figure 5: SA3-CASSCF(10,8)/6-31G* energy profiles for relaxed one-dimensional minimum-energy paths (MEPs) along the N1-H6 bond length (left) and the N1-C2-C3-C4 dihedral angle (right). The S_1 MEP is fully optimized with respect to the other coordinates, while the S_0 curve is obtained from single-point calculations.

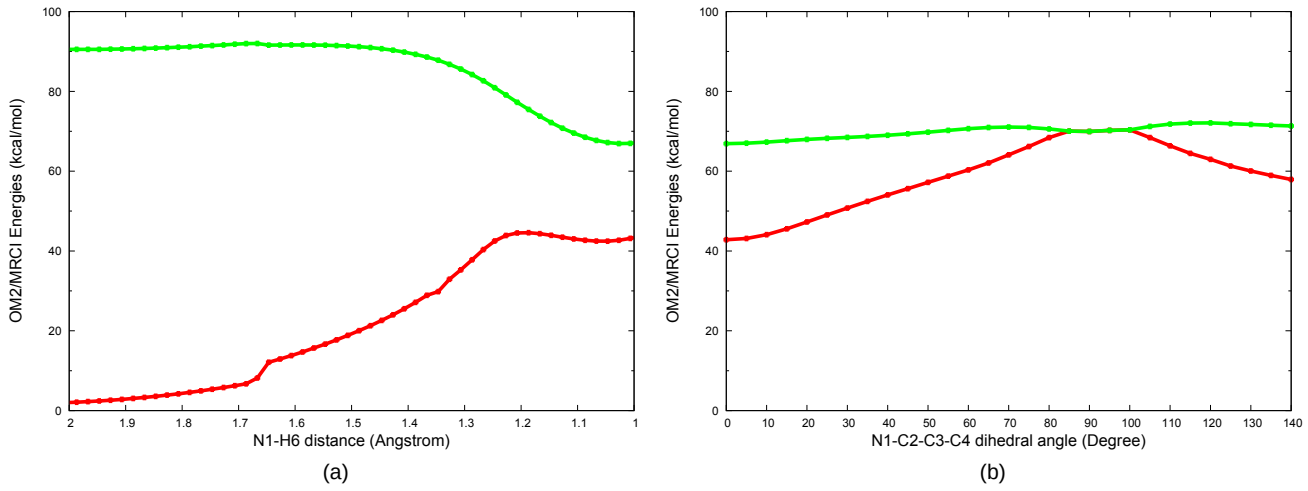

Figure 6: OM2/MRCI energy profiles for relaxed one-dimensional minimum-energy paths (MEPs) along the N1-H6 bond length (left) and the N1-C2-C3-C4 dihedral angle (right). The S_1 MEP is fully optimized with respect to the other coordinates, while the S_0 curve is obtained from single-point calculations.

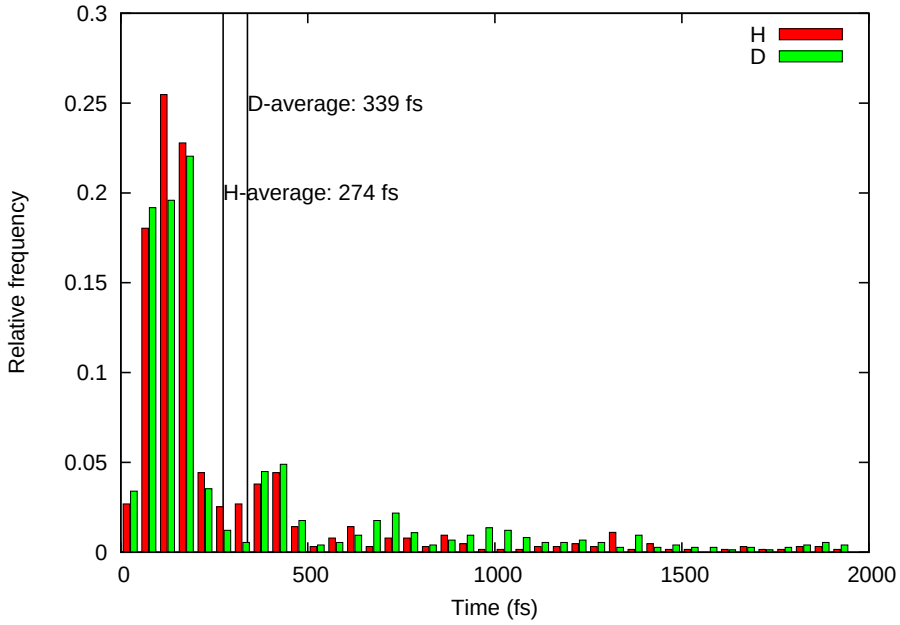

Figure 7: ESIPT time distribution for 7PyIn and 7PyIn-D (see text). The H/D isotope effect shifts this distribution towards longer times.

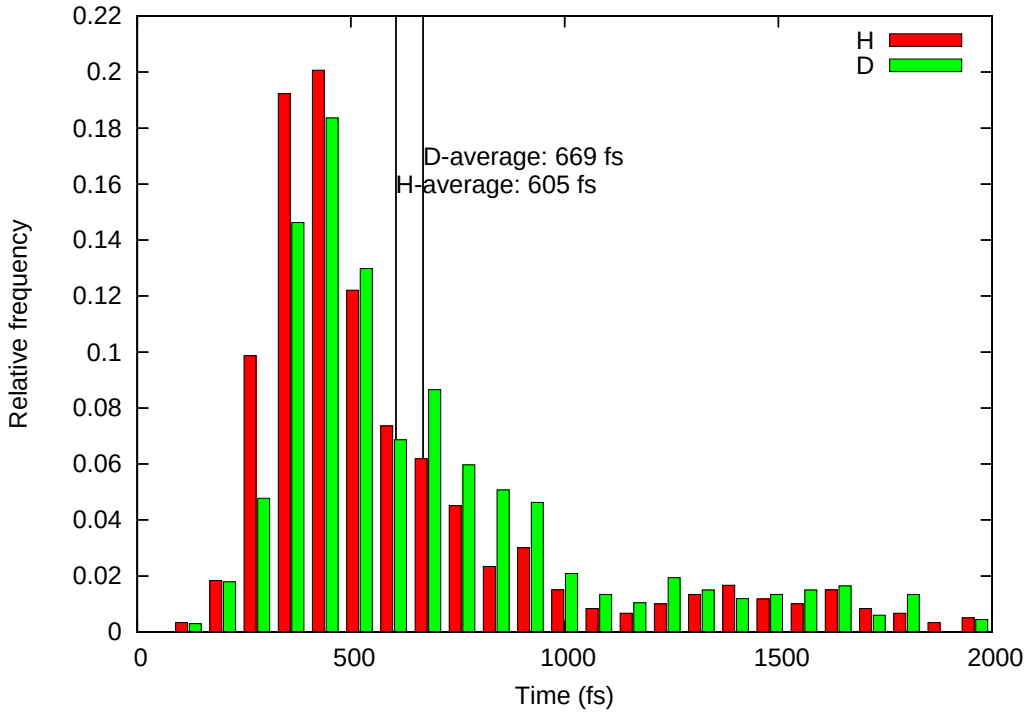

Figure 8: Time distributions of the $S_1 \rightarrow S_0$ internal conversion for 7PyIn and 7PyIn (D). The H/D isotope effect shifts this distribution towards longer times.

are shown in Fig. 7 along with their average values. These average ESIPT times change by less than 2 fs when applying the alternative criterion that the length of the forming N1-H6 bond drops below 1.1 Å. They are consistent with the measured spectroscopic data and isotope effects. Nosenko *et al.* attributed the first ion signal in their pump-probe REMPI spectra to the ESIPT process and determined its time to be 280 fs in 7PyIn and 390 fs in 7PyIn-D.[55] Both are close to our estimates of 274 fs [7PyIn] and 339 fs [7PyIn-D], respectively. In addition, we find that the peak of the ESIPT time distribution is shifted by ca. 50 fs when H is replaced by D, from ca. 150 fs (H, 26%) to ca. 200 fs (D, 22%).

Isotope effects are also seen in the distribution of the $S_1 \rightarrow S_0$ internal conversion time (see Fig. 8). Here the average hopping time is 64 fs longer for 7PyIn-D than for 7PyIn (669 fs vs. 605 fs). This indicates some correlation between the timing of proton transfer and internal conversion, the latter occurring on average about 330 fs after the former (for both isotomers).

The decomposition into different starting temperatures is shown for proton transfer in Fig. 9 and for internal conversion in Fig. 10. The average ESIPT times tend to increase with increasing temperature of the chosen temperature windows (7PyIn from 265 fs to 283 and 281 fs; 7PyIn-D from 301 fs to 381 and 410 fs), which has been rationalized in the main paper by the increased number of nonplanar starting geometries with out-of-plane distortions that are detrimental to the in-plane ESIPT process. The average hopping times seem to inherit this trend of increasing values (7PyIn from 597 fs to 628 and 582 fs; 7PyIn-D from 653 fs to 662 and 722 fs), but to

a lesser extent. The approach to the hopping point in the conical intersection region requires a rotation around the central C2-C3 bond (after ESIPT, see above), which may indeed be facilitated by out-of-plane distortions in the starting geometries that occur at higher temperatures. This may explain the decrease in the average internal conversion time that we find for 7PyIn in the highest temperature window.

8 Representative Trajectories

Fig. 11 (H) and 12 (D) show the time-dependent evolution of three key geometric parameters, the S_1/S_0 nonadiabatic coupling, and the S_1-S_0 energy gap during two typical trajectories. Both trajectories sample the same photophysical and photochemical events but at different times.

In the 7PyIn trajectory, the H6 atom is bound to the N5 atom for the first 180 fs, with a stable N1$\cdots$H6-N5 hydrogen bond (see Fig. 11). During this period, the S_1-S_0 energy gap is very large (more than 80 kcal/mol), the S_1/S_0 nonadiabatic coupling is small, and hence the excited-state decay is impossible. The excited-state proton transfer takes place at ca. 180 fs, which immediately yields a planar tautomer (syn-ht) with the N1-H6$\cdots$N5 hydrogen-bond pattern. After roaming in the resulting planar conformation for ca. 200 fs, the N1-C2-C3-C4 dihedral angle starts to twist, and the system then decays to the ground state via an S_1/S_0 conical intersection after ca. 800 fs. At this point, the nonadiabatic coupling is much larger (see top-right panel of Fig. 11). After ca. 100 fs of roaming in the S_0 state, the H6 atom returns to N5, with quick formation of the syn conformer (see N1-H6 and N5-H6) that triggers internal rotation around the central C2-C3 bond (see N1-C2-C3-C4) and a strong increase in the S_1-S_0 energy gap.

Similar dynamical features are observed for the deuterated isotopomer (see Fig. 12), albeit at different times. Here, the proton transfer happens after a much longer roaming period of 800 fs, possibly because of the more "damped" oscillations in the deuterium case (due to the higher mass). The excited-state decay occurs after another 200 fs at around 1000 fs, after some twist around the N1-C2-C3-C4 dihedral angle (see above) that should not be affected much by isotopic substitution. After the conversion to the ground state, the deuterium takes 250 fs for the transfer back to the initial position (syn conformer), which is again much longer than the 100 fs for the parent system. Isotope effects can thus generally be seen at the trajectory level for processes directly involving the H atom being replaced by D.

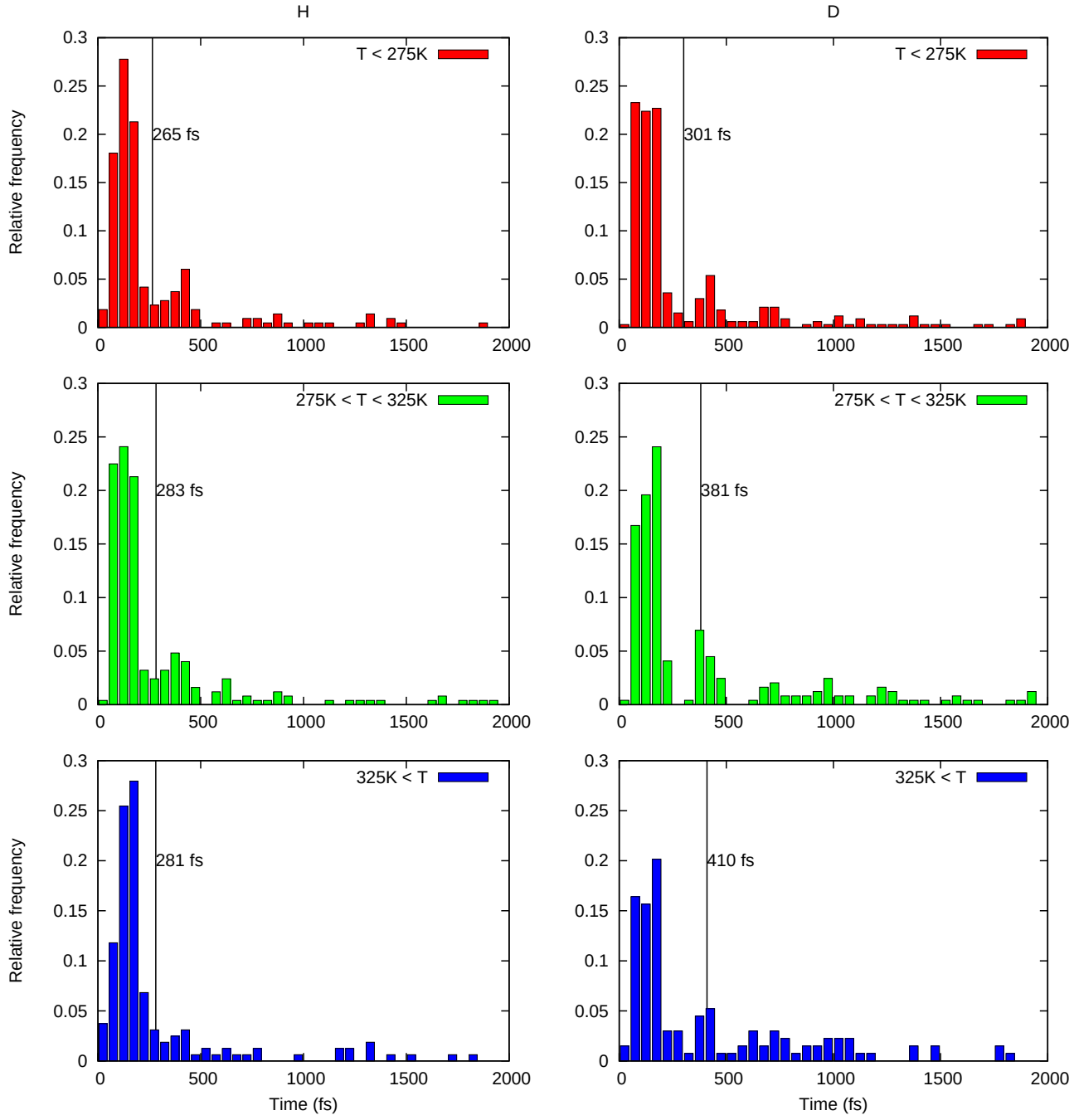

Figure 9: ESIPT time distributions in three temperature windows of initial conditions (top: less than 275 K; middle: between 275 and 325 K; bottom: larger than 325 K).

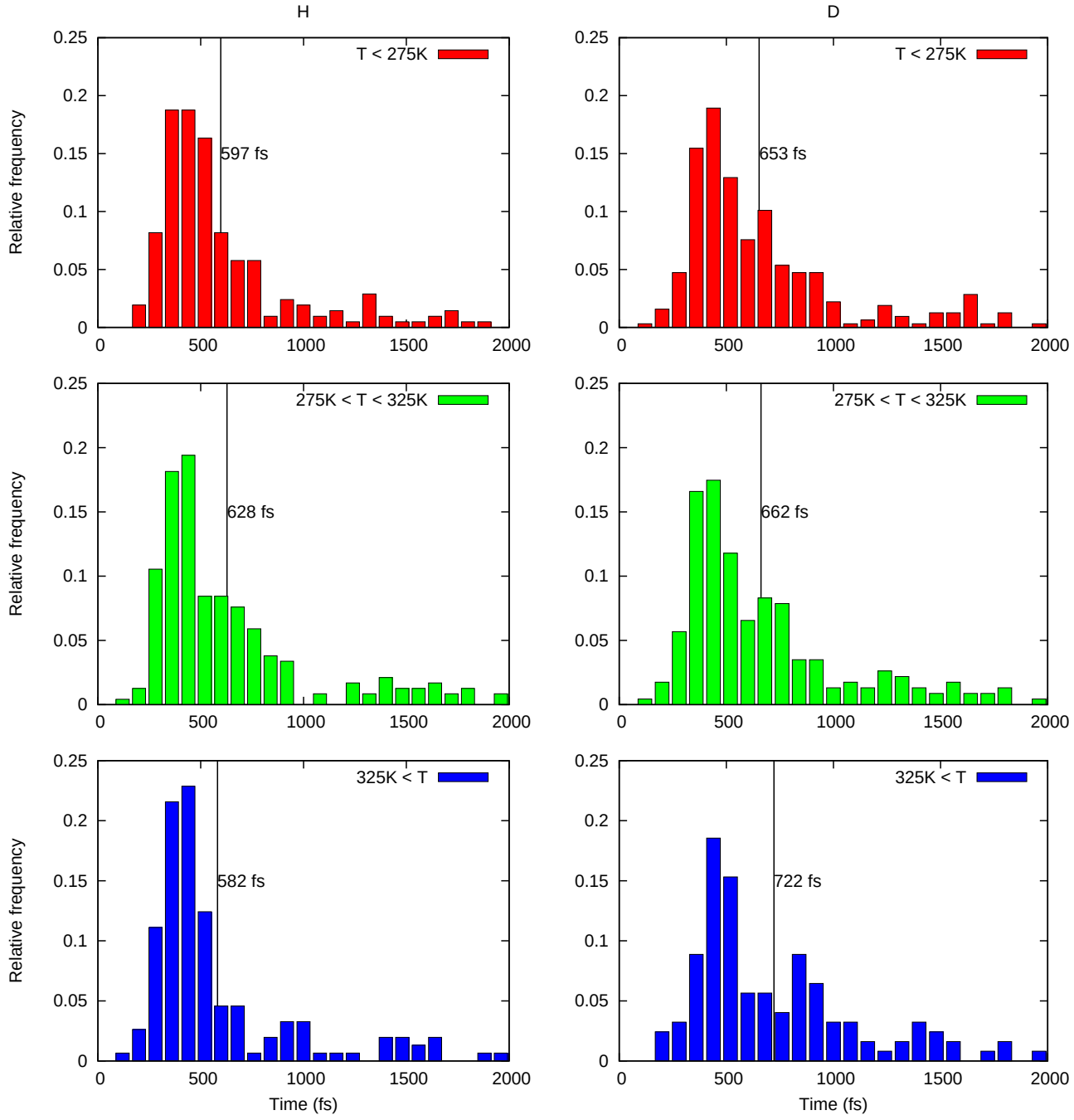

Figure 10: Hopping time distributions for the $S_1 \rightarrow S_0$ internal conversion in three temperature windows of initial conditions (top: less than 275 K; middle: between 275 and 325 K; bottom: greater than 325 K).

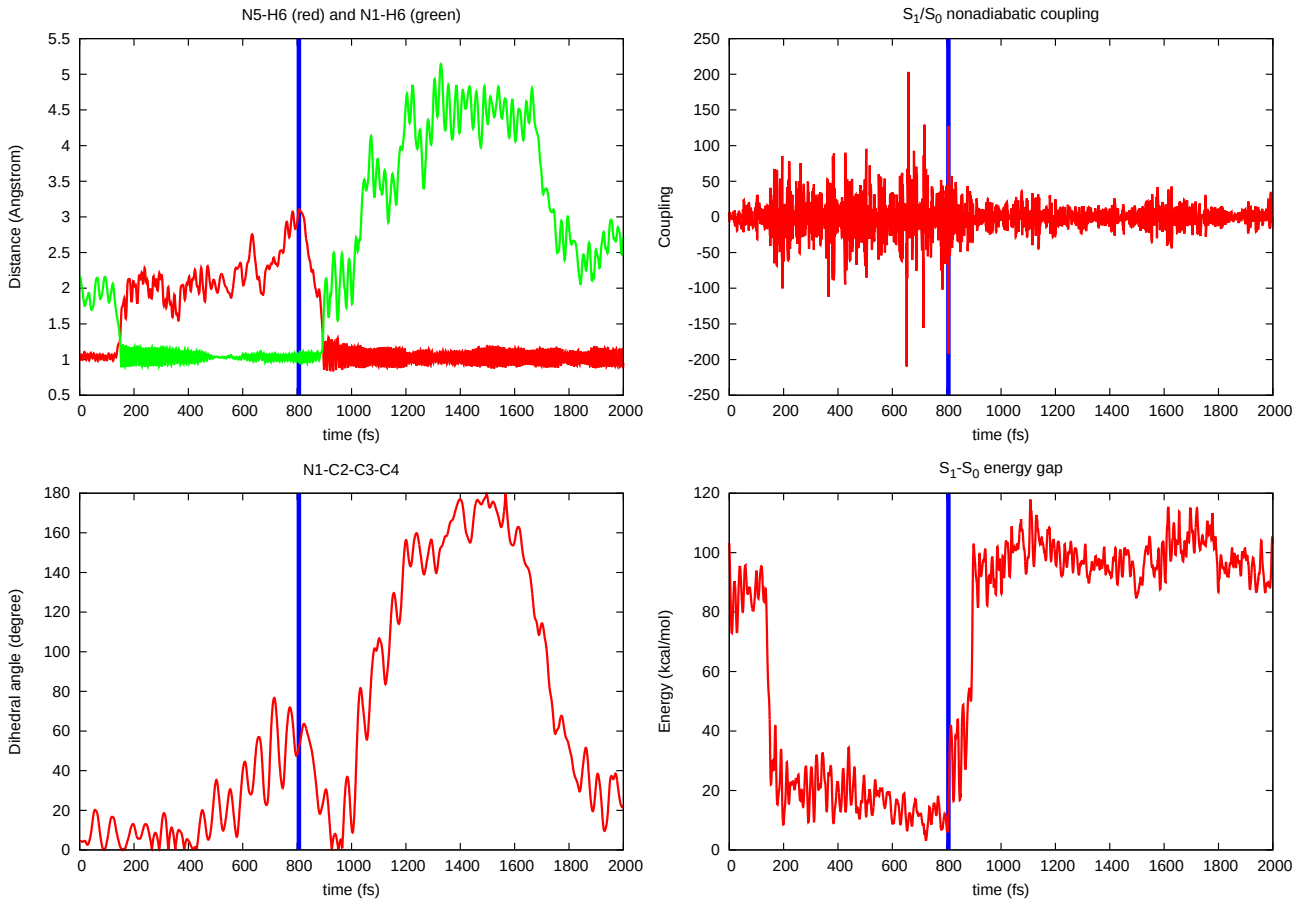

Figure 11: A typical trajectory for 7PyIn. The excited-state proton transfer and the $S_1 \rightarrow S_0$ internal conversion are completed after ca. 180 fs and after ca. 800 fs, respectively. In the S_0 state, the hydrogen atom is transferred back to the original donor atom. See the text for more detail.

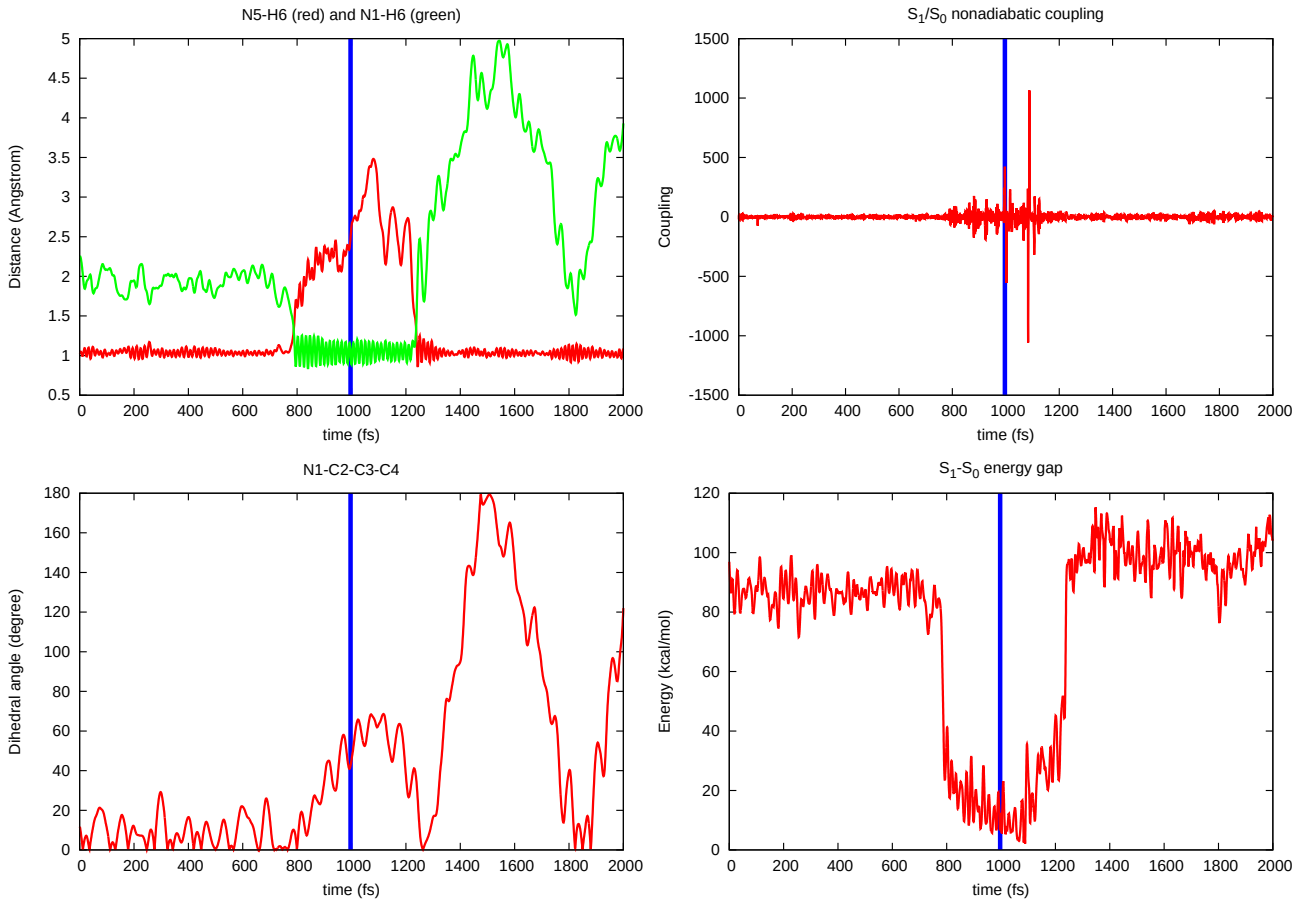

Figure 12: A typical trajectory for 7PyIn-D. The excited-state proton transfer and the $S_1 \rightarrow S_0$ internal conversion are completed after ca. 800 fs and after another 200 fs, respectively. In the S_0 state, the hydrogen atom is transferred back to the original donor atom. See the text for more detail.

9 Cartesian Coordinates of All Optimized Structures

9.1 DFT structures

S0-syn

C	-2.55874	0.04229	0.00000
C	-1.17352	-0.30344	0.00000
C	-0.13889	0.66235	0.00000
C	-0.56463	1.99877	0.00000
C	-1.92143	2.35885	0.00000
C	-2.92420	1.39586	0.00000
C	-3.29374	-1.19093	0.00000
C	-2.37086	-2.20501	0.00000
H	0.16899	2.79779	0.00000
H	-2.18472	3.41293	0.00000
H	-3.97164	1.68662	0.00000
H	-4.36902	-1.30477	0.00000
H	-2.51506	-3.27672	0.00000
C	1.29051	0.27786	0.00000
C	2.33178	1.22830	0.00000
C	3.65383	0.80466	0.00000
H	2.11163	2.28902	0.00000
C	2.85317	-1.43914	0.00000
C	3.93406	-0.56290	0.00000
H	4.45847	1.53531	0.00000
H	3.01687	-2.51579	0.00000
H	4.95256	-0.93793	0.00000
N	-1.09925	-1.67326	0.00000
N	1.57518	-1.04637	0.00000
H	-0.20126	-2.14128	0.00000

S0-syn-ht

C	-2.48414	0.54124	0.00094
C	-1.16892	-0.04729	0.00157
C	0.00706	0.75288	0.00192
C	-0.16358	2.15499	0.00176
C	-1.43608	2.72382	0.00114
C	-2.59703	1.93020	0.00071
C	-3.38196	-0.57361	0.00087
C	-2.58265	-1.70026	0.00113
H	0.70219	2.81101	0.00211
H	-1.53099	3.80613	0.00103
H	-3.57389	2.40950	0.00029
H	-4.46382	-0.54406	0.00055
H	-2.90158	-2.73682	0.00109
C	1.29639	0.10600	0.00241
C	2.56091	0.74030	0.00281
C	3.71934	-0.01143	0.00336
H	2.61042	1.82216	0.00268
C	2.41371	-2.00978	0.00311
C	3.65846	-1.42023	0.00349
H	4.68424	0.48760	0.00367
H	2.26594	-3.08469	0.00317
H	4.55520	-2.02873	0.00388
N	-1.23591	-1.40130	0.00162
N	1.29165	-1.26489	0.00261
H	0.26923	-1.69224	0.00209

S0-anti

C	-2.01092	1.50337	1.22617
C	-0.75754	0.82682	1.22130
C	0.01453	0.67282	0.05035
C	-0.53193	1.20093	-1.12387
C	-1.75941	1.88331	-1.13540
C	-2.50061	2.04785	0.02826
C	-2.52523	1.43017	2.56655
C	-1.61732	0.72644	3.30823
H	0.03016	1.07706	-2.04325
H	-2.12878	2.28982	-2.07287
H	-3.44998	2.57699	0.01254
H	-3.45630	1.84639	2.92594
H	-1.63486	0.44645	4.35245
C	1.33380	-0.00360	0.02020
C	2.23062	0.06169	1.10367
C	3.45743	-0.59169	1.01708
H	1.98889	0.65818	1.97780
C	2.83615	-1.27076	-1.18553
C	3.77161	-1.28674	-0.14904
H	4.16218	-0.54489	1.84341
H	3.04864	-1.78240	-2.12363
H	4.71414	-1.81363	-0.26202
N	-0.53901	0.37900	2.51194
N	1.65329	-0.65701	-1.11571
H	0.18793	-0.26622	2.77838

S0-anti-ht

C	-2.28684	1.13175	1.32294
C	-0.85850	0.80195	1.29970
C	-0.17800	0.68318	0.03570
C	-0.95391	0.89967	-1.14010
C	-2.30177	1.21038	-1.09187
C	-2.97864	1.32849	0.14201
C	-2.62965	1.16820	2.70867
C	-1.45829	0.87658	3.37524
H	-0.50460	0.82806	-2.12979
H	-2.84597	1.36585	-2.01928
H	-4.03894	1.57374	0.15036
H	-3.60087	1.37967	3.13711
H	-1.31638	0.81063	4.44969
C	1.21325	0.36219	-0.03375
C	2.04912	0.13721	1.10014
C	3.38115	-0.16705	0.94634
H	1.56472	0.22223	2.06975
C	3.16536	-0.05223	-1.42522
C	3.96928	-0.26783	-0.34078
H	3.99369	-0.33314	1.82804
H	3.50741	-0.10365	-2.45244
H	5.01727	-0.50674	-0.47628
N	-0.37793	0.65233	2.54174
N	1.84860	0.24794	-1.25429
H	1.29020	0.39864	-2.08404

9.2 OM2/MRCI Structures

S0-syn

C	-2.54958	0.04924	0.00000
C	-1.15601	-0.31744	0.00000
C	-0.13675	0.66312	0.00000
C	-0.55188	1.99858	0.00000
C	-1.90785	2.35267	0.00000
C	-2.91643	1.39866	0.00000
C	-3.29584	-1.17964	0.00000
C	-2.36239	-2.21322	0.00000
H	0.19343	2.80547	0.00000
H	-2.17245	3.41724	0.00000
H	-3.97197	1.68715	0.00000
H	-4.36863	-1.27832	0.00000
H	-2.56469	-3.27872	0.00000
C	1.29141	0.26992	0.00000
C	2.31671	1.23951	0.00000
C	3.64179	0.81660	0.00000
H	2.08510	2.30651	0.00000
C	2.84235	-1.44320	0.00000
C	3.91975	-0.54794	0.00000
H	4.45764	1.54794	0.00000
H	3.04761	-2.53054	0.00000
H	4.94886	-0.91073	0.00000
N	-1.08179	-1.69425	0.00000
N	1.57165	-1.04530	0.00000
H	-0.21997	-2.22023	0.00000

S0-anti

C	-2.00652	1.48573	1.22319
C	-0.74022	0.80546	1.21830
C	0.01408	0.69043	0.03535
C	-0.49862	1.27092	-1.12512
C	-1.73211	1.93901	-1.11470
C	-2.48255	2.07743	0.04594
C	-2.53397	1.37168	2.55708
C	-1.61282	0.63066	3.29121
H	0.07014	1.19495	-2.05608
H	-2.09795	2.37929	-2.04984
H	-3.42420	2.63476	0.05177
H	-3.46422	1.77726	2.91598
H	-1.69111	0.32856	4.33011
C	1.32379	-0.00875	-0.00476
C	2.24301	0.17941	1.04551
C	3.46608	-0.48190	0.98097
H	2.00883	0.83865	1.88110
C	2.76660	-1.40595	-1.12379
C	3.73768	-1.29707	-0.11651
H	4.21050	-0.35496	1.77386
H	2.97678	-2.04066	-2.00322
H	4.69414	-1.81510	-0.20421
N	-0.53244	0.29473	2.49085
N	1.59713	-0.77310	-1.07232
H	0.22545	-0.31106	2.76229

S0-anti-ht

C	-2.26721	1.12756	1.31653
C	-0.82625	0.79549	1.27164
C	-0.18207	0.68507	-0.00467
C	-0.97438	0.90405	-1.16334
C	-2.31843	1.21313	-1.08301
C	-2.98405	1.32894	0.15620
C	-2.58166	1.15779	2.71516
C	-1.39128	0.86272	3.36542
H	-0.51856	0.82992	-2.16943
H	-2.88836	1.37426	-2.00661
H	-4.05277	1.57535	0.18120
H	-3.54336	1.36693	3.15197
H	-1.25963	0.79937	4.44807
C	1.20588	0.36477	-0.07105
C	2.00102	0.14650	1.10785
C	3.32833	-0.15730	0.97722
H	1.49421	0.23624	2.06599
C	3.16207	-0.05019	-1.42273
C	3.93469	-0.26116	-0.29564
H	3.94486	-0.32563	1.86569
H	3.59349	-0.12189	-2.42983
H	4.99168	-0.50321	-0.39150
N	-0.33408	0.64432	2.50313
N	1.84171	0.25201	-1.28975
H	1.29392	0.40305	-2.13891

S1S0

C	-2.55664	0.12056	0.13455
C	-1.16472	-0.27164	0.19207
C	-0.17742	0.63449	-0.19204
C	-0.57133	1.90677	-0.65176
C	-1.91561	2.27452	-0.68642
C	-2.92647	1.39335	-0.29360
C	-3.27552	-1.04176	0.56156
C	-2.26187	-2.03450	0.85166
H	0.19702	2.61978	-0.96198
H	-2.18429	3.27774	-1.03428
H	-3.97624	1.69666	-0.31129
H	-4.34743	-1.16551	0.63895
H	-2.50136	-3.03325	1.22160
C	1.25585	0.28706	-0.08672
C	1.98143	0.48480	1.08195
C	3.32449	0.09764	1.13446
H	1.49594	0.94145	1.94723
C	3.14042	-0.76853	-1.12042
C	3.88973	-0.54341	0.01964
H	3.91827	0.27119	2.03079
H	3.55061	-1.30224	-1.98461
H	4.92853	-0.88849	0.05566
N	-1.04209	-1.59490	0.65273
N	1.83767	-0.30976	-1.19479
H	1.21510	-0.74205	-1.87861

S1-syn

C	-2.55177	0.06588	0.00000
C	-1.15455	-0.25759	0.00000
C	-0.11746	0.69817	0.00000
C	-0.58580	2.05208	0.00000
C	-1.93649	2.37081	0.00000
C	-2.95447	1.40935	0.00000
C	-3.24126	-1.17833	0.00000
C	-2.23551	-2.22425	0.00000
H	0.15513	2.85975	0.00000
H	-2.22686	3.43059	0.00000
H	-4.00946	1.68479	0.00000
H	-4.30991	-1.35092	0.00000
H	-2.43903	-3.29162	0.00000
C	1.25893	0.28454	0.00000
C	2.32335	1.23488	0.00000
C	3.62459	0.77412	0.00000
H	2.10741	2.30692	0.00000
C	2.76969	-1.47305	0.00000
C	3.87164	-0.60551	0.00000
H	4.46673	1.47860	0.00000
H	2.96183	-2.56804	0.00000
H	4.89024	-0.99226	0.00000
N	-1.02920	-1.66205	0.00000
N	1.50931	-1.06294	0.00000
H	-0.08700	-2.09085	-0.00000

S1-syn-ht

C	-2.50247	0.59379	0.00094
C	-1.22815	-0.06913	0.00150
C	-0.02876	0.66456	0.00187
C	-0.15850	2.06361	0.00172
C	-1.40806	2.70104	0.00119
C	-2.59689	1.99089	0.00077
C	-3.46637	-0.45544	0.00076
C	-2.69226	-1.69697	0.00116
H	0.73948	2.69204	0.00202
H	-1.43570	3.79785	0.00111
H	-3.56976	2.48793	0.00032
H	-4.54514	-0.37262	0.00042
H	-3.16305	-2.68257	0.00111
C	1.29395	0.01008	0.00241
C	2.49000	0.72755	0.00282
C	3.71861	0.06452	0.00337
H	2.47364	1.82407	0.00270
C	2.55294	-2.04841	0.00313
C	3.73949	-1.34520	0.00353
H	4.65225	0.62528	0.00366
H	2.53491	-3.14587	0.00325
H	4.69410	-1.87932	0.00396
N	-1.41142	-1.48363	0.00157
N	1.34951	-1.37903	0.00258
H	0.48182	-1.91453	0.00215

S1-anti

C	-2.00672	1.52950	1.21323
C	-0.73156	0.85956	1.25196
C	0.04404	0.64643	0.08904
C	-0.56392	1.10783	-1.13587
C	-1.78798	1.74882	-1.16137
C	-2.52590	2.01029	0.00351
C	-2.51608	1.52778	2.54425
C	-1.57169	0.82895	3.35072
H	-0.01739	0.91415	-2.06052
H	-2.19760	2.07968	-2.12322
H	-3.47560	2.54859	-0.02579
H	-3.44387	1.95605	2.89692
H	-1.64740	0.64784	4.41853
C	1.33312	0.01402	0.04353
C	2.18064	-0.11674	1.18591
C	3.39466	-0.76489	1.04617
H	1.91962	0.34627	2.14335
C	2.90147	-1.04173	-1.29195
C	3.77004	-1.26569	-0.20441
H	4.06758	-0.87940	1.90669
H	3.21494	-1.39973	-2.29408
H	4.72560	-1.77032	-0.34213
N	-0.53575	0.43781	2.57538
N	1.73916	-0.42820	-1.18744
H	0.24809	-0.12651	2.89053

S1-anti-ht

C	-2.27812	1.13038	1.29381
C	-0.87721	0.80777	1.25638
C	-0.19727	0.68879	0.02918
C	-0.96560	0.90448	-1.12703
C	-2.33325	1.22011	-1.07858
C	-3.01442	1.33883	0.11899
C	-2.61500	1.16354	2.67463
C	-1.37196	0.85249	3.38619
H	-0.50556	0.83073	-2.12278
H	-2.86807	1.37564	-2.02388
H	-4.07810	1.58363	0.16023
H	-3.57650	1.37255	3.12403
H	-1.31719	0.80397	4.47578
C	1.23778	0.35842	-0.02709
C	2.02838	0.14632	1.10281
C	3.38282	-0.16525	0.96016
H	1.58706	0.22408	2.09282
C	3.16669	-0.05440	-1.43883
C	3.95243	-0.26383	-0.32206
H	4.00117	-0.33125	1.84243
H	3.57303	-0.12654	-2.45481
H	5.01274	-0.50619	-0.44026
N	-0.37527	0.64831	2.58110
N	1.83132	0.25389	-1.28423
H	1.26987	0.39157	-2.11941

9.3 CASSCF Structures

S0-syn

C	-2.53200	0.03920	0.00000
C	-1.18041	-0.31549	0.00000
C	-0.13840	0.65300	0.00000
C	-0.55709	1.97540	0.00000
C	-1.92132	2.34336	0.00000
C	-2.90163	1.39669	0.00000
C	-3.28577	-1.18303	0.00000
C	-2.38428	-2.18916	0.00000
H	0.16396	2.76956	0.00000
H	-2.17500	3.38826	0.00000
H	-3.94022	1.67749	0.00000
H	-4.35198	-1.28331	0.00000
H	-2.53914	-3.24851	0.00000
C	1.30160	0.27055	0.00000
C	2.33544	1.22512	0.00000
C	3.64308	0.81590	0.00000
H	2.11402	2.27287	0.00000
C	2.86370	-1.42587	0.00000
C	3.93194	-0.54768	0.00000
H	4.43572	1.54260	0.00000
H	3.02648	-2.48894	0.00000
H	4.94272	-0.91027	0.00000
N	-1.11863	-1.67633	0.00000
N	1.58865	-1.03171	0.00000
H	-0.26133	-2.17667	0.00000

S1-syn

C	-2.56148	0.04118	-0.00000
C	-1.16912	-0.28549	0.00000
C	-0.09237	0.70508	0.00000
C	-0.56791	2.03444	0.00000
C	-1.95583	2.34066	0.00000
C	-2.94553	1.37334	-0.00000
C	-3.26570	-1.21936	0.00000
C	-2.32959	-2.18113	0.00000
H	0.12291	2.85192	0.00000
H	-2.24252	3.37642	0.00000
H	-3.98214	1.65553	-0.00000
H	-4.32670	-1.35848	0.00000
H	-2.42481	-3.24584	-0.00000
C	1.27928	0.29322	0.00000
C	2.35210	1.22906	0.00000
C	3.66021	0.79058	-0.00000
H	2.15006	2.28424	0.00000
C	2.80342	-1.44973	0.00000
C	3.89682	-0.61975	-0.00000
H	4.47351	1.49296	-0.00000
H	2.96369	-2.51742	0.00000
H	4.89077	-1.02531	-0.00000
N	-1.06454	-1.59433	0.00000
N	1.53295	-1.07717	0.00000
H	-0.13734	-2.00158	0.00000

S1S0

C	-2.56806	-0.06206	0.05024
C	-1.18894	-0.37163	0.05226
C	-0.21641	0.60187	-0.12555
C	-0.69135	1.89244	-0.33743
C	-2.05518	2.22089	-0.33419
C	-3.01017	1.25511	-0.14163
C	-3.21162	-1.28415	0.26276
C	-2.13556	-2.26903	0.38444
H	0.02498	2.67390	-0.51042
H	-2.34506	3.24208	-0.49988
H	-4.05777	1.49502	-0.14348
H	-4.26253	-1.48332	0.32061
H	-2.27867	-3.31961	0.55145
C	1.23353	0.29330	-0.01890
C	2.04950	0.91898	0.87402
C	3.45127	0.63312	0.92905
H	1.62275	1.64132	1.54612
C	3.10728	-0.97288	-0.85060
C	3.94253	-0.35614	0.03156
H	4.08865	1.11272	1.64505
H	3.44834	-1.71111	-1.54998
H	4.98343	-0.62565	0.03486
N	-0.97537	-1.75239	0.26867
N	1.74454	-0.62025	-0.97694
H	1.15082	-1.41576	-1.09263

References

[1] W. Weber. PhD thesis, University of Zürich, 1996.

[2] W. Weber and W. Thiel. Orthogonalization corrections for semiempirical methods. *Theor. Chem. Acc.*, 103:495–506, 2000.

[3] A. Koslowski, M.E. Beck, and W. Thiel. Implementation of a general multireference configuration interaction procedure with analytic gradients in a semiempirical context using the graphical unitary group approach. *J. Comput. Chem.*, 24:714–726, 2003.

[4] W. Thiel. MNDO99 program, version 6.1, 2007. Max-Planck-Institut für Kohlenforschung, Mülheim, Germany, 2007.

[5] T.W. Keal, A. Koslowski, and W. Thiel. Comparison of algorithms for conical intersection optimisation using semiempirical methods. *Theor. Chem. Acc.*, 118:837–844, 2007.

[6] M.J.S. Dewar, J.A. Hashmall, and C.G. Venier. Ground states of conjugated molecules. IX. Hydrocarbon radicals and radical ions. *J. Am. Chem. Soc.*, 90:1953–1957, 1968.

[7] M.R. Silva-Junior and W. Thiel. Benchmark of Electronically Excited States for Semiempirical Methods: MNDO, AM1, PM3, OM1, OM2, OM3, INDO/S, and INDO/S2. *J. Chem. Theory Comput.*, 6:1546–1564, 2010.

[8] E. Fabiano and W. Thiel. Nonradiative deexcitation dynamics of 9H-adenine: An OM2 surface hopping study. *J. Phys. Chem. A*, 112:6859–6863, 2008.

[9] Z.G. Lan, E. Fabiano, and W. Thiel. Photoinduced Nonadiabatic Dynamics of Pyrimidine Nucleobases: On-the-Fly Surface-Hopping Study with Semiempirical Methods. *J. Phys. Chem. B*, 113:3548–3555, 2009.

[10] Z.G. Lan, E. Fabiano, and W. Thiel. Photoinduced Nonadiabatic Dynamics of 9H-Guanine. *ChemPhysChem*, 10:1225–1229, 2009.

[11] Z.G. Lan, Y. Lu, E. Fabiano, and W. Thiel. QM/MM Nonadiabatic Decay Dynamics of 9H-Adenine in Aqueous Solution. *ChemPhysChem*, 12:1989–1998, 2011.

[12] Y. Lu, Z.G. Lan, and W. Thiel. Hydrogen Bonding Regulates the Monomeric Nonradiative Decay of Adenine in DNA Strands. *Angew. Chem. Int. Ed.*, 50:6864–6867, 2011.

[13] O. Weingart, Z.G. Lan, A. Koslowski, and W. Thiel. Chiral Pathways and Periodic Decay in cis-Azobenzene Photodynamics. *J. Phys. Chem. Lett.*, 2:1506–1509, 2011.

[14] A. Kazaryan, Z.G. Lan, L.V. Schäfer, W. Thiel, and M. Filatov. Surface Hopping Excited-State Dynamics Study of the Photoisomerization of a Light-Driven Fluorene Molecular Rotary Motor. *J. Chem. Theory Comput.*, 7:2189–2199, 2011.

[15] Z.G. Lan, Y. Lu, O. Weingart, and W. Thiel. Nonadiabatic Decay Dynamics of a Benzylidene Malononitrile. *J. Phys. Chem. A*, 116:1510–1518, 2012.

[16] Y. Lu, Z.G. Lan, and W. Thiel. Monomeric adenine decay dynamics influenced by the DNA environment. *J. Comput. Chem.*, 33:1225–1235, 2012.

[17] G.L. Cui, Z.G. Lan, and W. Thiel. Intramolecular hydrogen bonding plays a crucial role in the photophysics and photochemistry of the GFP chromophore. *J. Am. Chem. Soc.*, 134:1662–1672, 2012.

[18] G.L. Cui and W. Thiel. Nonadiabatic dynamics of a truncated indigo model. *Phys. Chem. Chem. Phys.*, 14:12378–12384, 2012.

[19] G.L. Cui and W. Thiel. Photoinduced Ultrafast Wolff Rearrangement: A Non-Adiabatic Dynamics Perspective. *Angew. Chem. Int. Ed.*, 52:433–436, 2013.

[20] L. Spörkel, G.L. Cui, and W. Thiel. Photodynamics of Schiff base salicylideneaniline: Trajectory surface-hopping simulations. *J. Phys. Chem. A*, 117:4574–4583, 2013.

[21] A.D. Becke. Density-functional exchange-energy approximation with correct asymptotic behavior. *Phys. Rev. A*, 38:3098–3100, 1988.

[22] C. Lee, W.T. Yang, and R.G. Parr. Development of the Colle-Salvetti correlation-energy formula into a functional of the electron density. *Phys. Rev. B*, 37:785–789, 1988.

[23] A.D. Becke. A new mixing of Hartree-Fock and local density-functional theories. *J. Chem. Phys.*, 98:1372–1377, 1993.

[24] R. Ditchfield, W.J. Hehre, and J.A. Pople. Self-Consistent Molecular-Orbital Methods. IX. An Extended Gaussian-Type Basis for Molecular-Orbital Studies of Organic Molecules. *J. Chem. Phys.*, 54:724–728, 1971.

[25] T. Yanai, D.P. Tew, and N.C. Handy. A new hybrid exchange-correlation functional using the Cooulomb-attenuated method CAM-B3LYP. *Chem. Phys. Lett.*, 393:51–57, 2004.

[26] T.H. Dunning Jr. Gaussian basis sets for use in correlated molecular calculations. I. The atoms boron through neon and hydrogen. *J. Chem. Phys.*, 90:1007–1023, 1989.

[27] S. Grimme and M. Waletzke. A combination of Kohn–Sham density functional theory and multi-reference configuration interaction methods. *J. Chem. Phys.*, 111:5645–5655, 1999.

[28] A. Schäfer, H. Horn, and R. Ahlrichs. Fully optimized contracted Gaussian basis sets for atoms Li to Kr. *J. Chem. Phys.*, 97:2571–2577, 1992.

[29] A. Schäfer, C. Huber, and R. Ahlrichs. Fully optimized contracted Gaussian basis sets of triple zeta valence quality for atoms Li to Kr. *J. Chem. Phys.*, 100:5829–5835, 1994.

[30] K. Andersson, P.Å. Malmqvist, and B.O. Roos. Second-order perturbation theory with a complete active space self-consistent field reference function. *J. Chem. Phys.*, 96:1218, 1992.

[31] N. Försberg and P.Å. Malmqvist. Multiconfiguration perturbation theory with imaginary level shift. *Chem. Phys. Lett.*, 274:196–204, 1997.

[32] ChemShell3.4, a Computational Chemistry Shell, see www.chemshell.org.

[33] M.J. Frisch, G.W. Trucks, H.B. Schlegel, G.E. Scuseria, M.A. Robb, J.R. Cheesem, G. Scalmani, V. Barone, B. Mennucci, G.A. Petersson, H. Nakatsuji, M. Caricato, X. Li, H.P. Hratchian, A.F. Izmaylov, J. Bloino, G. Zheng, J.L. Sonnenberg, M. Hada, M. Ehara, K. Toyota, R. Fukuda, J. Hasegawa, M. Ishida, T. Nakajima, Y. Honda, O. Kitao, H. Nakai, T. Vreven, J.A. Montgomery Jr., J.E. Peralta, F. Ogliaro, M. Bearpark, J.J. Heyd, E. Brothers, K.N. Kudin, V.N. Staroverov, R. Kobayashi, J. Normand, K. Raghavachari, A. Rendell, J.C. Burant, S.S. Iyengar, J. Tomasi, M. Cossi, N. Rega, J.M. Millam, M. Klene, J.E. Knox, J.B. Cross, V. Bakken, C. Adamo, J. Jaramillo, R. Gomperts, R.E. Stratmann, O. Yazyev, A.J. Austin, R. Cammi, C. Pomelli, J.W. Ochterski, R.L. Martin, K. Morokuma, V.G. Zakrzewski, G.A. Voth, P. Salvador, J.J. Dannenberg, S. Dapprich, A.D. Daniels, Ö. Farkas, J.B. Foresman, J.V. Ortiz, J. Cioslowski, and D.J. Fox. Gaussian 09, Revision B.01. Gaussian, Inc., Wallingford CT, 2010.

[34] G. Karlström, R. Lindh, P.Å. Malmqvist, B.O. Roos, U. Ryde, V. Veryazov, P.O. Widmark, M. Cossi, B. Schimmelpfennig, P. Neogrady, and L. Seijo. MOLCAS: a program package for computational chemistry. *Comput. Mater. Sci.*, 28:222–229, 2003.

[35] F. Aquilante, L. De Vico, N. Ferré, G. Ghigo, P. Malmqvist, P. Neogrády, T.B. Pedersen, M. Pitoňák, M. Reiher, B.O. Roos, L. Serrano-Andrès, M. Urban, V. Veryazov, and R. Lindh. MOLCAS 7: the next generation. *J. Comput. Chem.*, 31:224–247, 2010.

[36] TURBOMOLE V5.7.1 2004, a development of University of Karlsruhe and Forschungszentrum Karlsruhe GmbH, 1989-2007, TURBOMOLE GmbH, since 2007; available from `http://www.turbomole.com`.

[37] E. Wigner. On the quantum correction for thermodynamic equilibrium. *Phys. Rev.*, 40:749–759, 1932.

[38] M. Barbatti, G. Granucci, M. Persico, M. Ruckenbauer, M. Vazdar, M. Eckert-Maksić, and H. Lischka. The on-the-fly surface-hopping program system Newton-X: Application to ab initio simulation of the nonadiabatic photodynamics of benchmark systems. *J. Photochem. Photobiol. A*, 190:228–240, 2007.

[39] G. Bussi, D. Donadio, and M. Parrinello. Canonical sampling through velocity rescaling. *J. Chem. Phys.*, 126:14101–14107, 2007.

[40] H.J.C. Berendsen, J.P.M. Postma, W.F. van Gunsteren, A. DiNola, and J.R. Haak. Molecular dynamics with coupling to an external bath. *J. Chem. Phys.*, 81:3684–3690, 1984.

[41] H.C. Andersen. Molecular dynamics simulations at constant pressure and/or temperature. *J. Chem. Phys.*, 72:2384–2393, 1980.

[42] S. Nose. A unified formulation of the constant temperature molecular dynamics methods. *J. Chem. Phys.*, 81:511–519, 1984.

[43] W.G. Hoover. Canonical dynamics: Equilibrium phase-space distributions. *Phys. Rev. A*, 31:1695–1697, 1985.

[44] G.J. Martyna, M.L. Klein, and M. Tuckerman. Nose-Hoover chains: The canonical ensemble via continuous dynamics. *J. Chem. Phys.*, 97:2635–2643, 1992.

[45] T. Schneider and E. Stoll. Molecular-dynamics study of a three-dimensional one-component model for distortive phase transitions. *Phys. Rev. B*, 17:1302–1322, 1978.

[46] N. Otte, M. Scholten, and W. Thiel. Looking at Self-Consistent-Charge Density Functional Tight Binding from a Semiempirical Perspective. *J. Phys. Chem. A*, 111:5751–5755, 2007.

[47] M. Elstner, D. Porezag, G. Jungnickel, J. Elsner, M. Haugk, Th. Frauenheim, S. Suhai, and G. Seifert. Self-consistent-charge density-functional tight-binding method for simulations of complex materials properties. *Phys. Rev. B*, 58:7260–7268, 1998.

[48] Q. Cui, M. Elstner, E. Kaxiras, T. Frauenheim, and M. Karplus. A QM/MM Implementation of the Self-Consistent Charge Density Functional Tight Binding (SCC-DFTB) Method. *J. Phys. Chem. B*, 105:569–585, 2001.

[49] J.C. Tully. Molecular dynamics with electronic transitions. *J. Chem. Phys.*, 93:1061–1071, 1990.

[50] S. Hammes-Schiffer and J.C. Tully. Proton transfer in solution: Molecular dynamics with quantum transitions. *J. Chem. Phys.*, 101:4657–4667, 1994.

[51] E. Fabiano, T.W. Keal, and W. Thiel. Implementation of surface hopping molecular dynamics using semiempirical methods. *Chem. Phys.*, 349:334–347, 2008.

[52] T.W. Keal, M. Wanko, and W. Thiel. Assessment of semiempirical methods for the photoisomerisation of a protonated Schiff base. *Theor. Chem. Acc.*, 123:145–156, 2009.

[53] G. Granucci, M. Persico, and A. Zoccante. Including quantum decoherence in surface hopping. *J. Chem. Phys.*, 133:134111, 2010.

[54] A.L. Sobolewski and W. Domcke. Computational studies of the photophysics of hydrogen-bonded molecular systems. *J. Phys. Chem. A*, 111:11725–11735, 2007.

[55] Y. Nosenko, G. Wiosna-Sałyga, M. Kunitski, I. Petkova, A. Singh, W.J. Buma, R.P. Thummel, B. Brutschy, and J. Waluk. Proton transfer with a twist? Femtosecond Dynamics of 7-(2-pyridyl) indole in Condensed Phase and in Supersonic Jets. *Angew. Chem. Int. Ed.*, 47:6037–6040, 2008.